Journal of Alloys and Compounds 520 (2012) 174–179

Contents lists available at SciVerse ScienceDirect

Journal of Alloys and Compounds

journal homepage: www.elsevier.com/locate/jallcom

Low-temperature structure and lattice dynamics of the thermoelectric clathrate $Sn_{24}P_{19.3}I_8$

Vladimir V. Novikov[a], Alexander V. Matovnikov[a], Dmitrii V. Avdashchenko[a], Nikolai V. Mitroshenkov[a], Evgeny Dikarev[b], Satoshi Takamizawa[c], Maria A. Kirsanova[d], Andrei V. Shevelkov[d,*]

[a] General Physics Department, Bryansk State University, Russia
[b] Department of Chemistry, University at Albany, Albany, NY, USA
[c] Department of Nanosystem Science, Yokohama City University, Yokohama, Japan
[d] Chemistry Department, Lomonosov Moscow State University, Moscow, Russia

ARTICLE INFO

Article history:
Received 26 October 2011
Received in revised form
29 December 2011
Accepted 31 December 2011
Available online 9 January 2012

Keywords:
Clathrates
Thermoelectric materials
Crystal structure
Lattice dynamics
Heat capacity

ABSTRACT

The crystal structure of the thermoelectric clathrate $Sn_{24}P_{19.3}I_8$ was determined down to 10 K showing no variations with the temperature. Even at 10 K $Sn_{24}P_{19.3}I_8$ crystallizes in the type-I clathrate structure, space group Pm3-n, with the cubic unit cell parameter ranging from 10.9173 Å at 10 K to 10.9554 Å at room temperature. In its crystal structure, tin and phosphorus atoms form the framework that traps the guest iodine atoms in the polyhedral cavities of two different shapes. The temperature-dependent crystal structure data and the results of the heat capacity measurements revealed the localized vibrations of the guest atoms inside the oversized cavities with the characteristic Einstein temperatures of $\theta_{E1} = 60$ K and $\theta_{E2} = 78$ K, whereas the characteristic Debye temperature for $Sn_{24}P_{19.3}I_8$ is 265 K. The room temperature lattice thermal conductivity was calculated using the Debye model to be $\kappa_L = 0.85\ W\,m^{-1}\,K^{-1}$, which is in excellent agreement with the experimentally measured data and demonstrates that the thermal conductivity is almost entirely phononic.

1. Introduction

Thermoelectric materials that convert thermal energy to electrical and vice versa attract great attention in the last 20 years. It is generally believed that new and improved thermoelectric materials will find their applications in waste heat conversion, direct solar thermal energy conversion, and cryogenic cooling [1–3]. The quality of a thermoelectric material is measured by its figure-of-merit $ZT = TS^2\sigma/\kappa$, which relates a dimensionless factor ZT to the square of the Seebeck coefficient (S), the absolute temperature (T), the electrical conductivity (σ), and the thermal conductivity (κ). The product $S^2\sigma$ known as the power factor characterizes the transport of the charge carriers, which is the highest for narrow-gap or degenerate semiconductors. Then, the task for the chemists and materials scientists is to create a semiconductor having a very low thermal conductivity. This problem is tackled in different ways. The proposed solutions include various kinds of nanostructuring [4,5], building materials from heavy elements [6], introducing a severe disorder into the crystal structure of a material [7,8], and employing the localized vibrations of atoms trapped inside the oversized cages. For the latter solution, two types of cage compounds are commonly used: filled skutterudites [9] and clathrates [10].

Clathrates are the family of inclusion compounds that possess crystal structures built on trapping guest ions inside large cavities of a framework composed mainly from atoms of the group 14 elements. Though there are nine clathrate types classified by Jeffrey [11] and the tenth type has been recently discovered [12], the type-I clathrates are by far the most abundant and demonstrate the most interesting thermoelectric properties [13]. Depending on the charge of the framework, the type-I clathrates are subdivided into anionic and cationic ones. In the latter type, halogen or tellurium anions serve as guests, which compensate for the positive charge smeared over the framework atoms [10]. Cationic clathrates, also known as inversed clathrates, have been studied less intensively compared to their anionic counterparts. About 30 type-I cationic clathrates have been synthesized and structurally characterized. It was shown that cationic clathrates behave differently, mainly depending on the nature of the group 14 elements composing the framework. Silicon-based cationic type-I clathrates display utmost chemical and thermal stability and behave as poor metals or heavily doped semiconductors though their thermal conductivity reaches relatively high room-temperature values of 3–4 $W\,m^{-1}\,K^{-1}$

* Corresponding author at: Chemistry Department, Lomonosov Moscow State University, Leninskie Gory 1-3, Moscow 119991, Russia. Tel.: +7 495 939 4788.
E-mail address: shev@inorg.chem.msu.ru (A.V. Shevelkov).

0925-8388/$ – see front matter © 2012 Elsevier B.V. All rights reserved.
doi:10.1016/j.jallcom.2011.12.171

[14,15]. Much lower thermal conductivity (below $1\,W\,m^{-1}\,K^{-1}$) was reported for the Ge-based clathrates in the Ge–P–Te system. While these compounds were shown to possess less promising electrical transport properties, their structural flexibility implies that fine tuning of the power factor is possible by means of various substitutions both at the framework and guest positions [16,17]. Tin-based cationic type-I clathrates display even lower thermal conductivity ranging from 0.4 to $1.6\,W\,m^{-1}\,K^{-1}$ at 298 K [8,18–21]. These compounds behave as inverted Zintl phases [22] and display properties of typical narrow-gap semiconductors with the room-temperature electrical conductivity reaching $10^3\,S\,m^{-1}$. As a consequence, the electronic contribution to the total thermal conductivity is negligible, and the thermal conductivity is almost entirely phononic. Its low values are attributed to the motion (rattling) of the guest atoms inside the oversized cages [23,24].

The goal of this research was to determine the crystal structure of $Sn_{24}P_{19.3}I_8$ at cryogenic temperatures, and to use the structural data along with the results of the heat capacity measurements for investigation of the clathrate lattice dynamics. Herein we report that the Einstein contributions to the heat capacity characterize the localized vibrations of the guest atoms inside the cavities of the framework. We also demonstrate that thermal conductivity of $Sn_{24}P_{19.3}I_8$ can be described as the dominant contribution of the lattice part arising from the localized motion of the guest atoms.

2. Experimental

2.1. Sample preparation and characterization

Tin powder (99.99%), red phosphorus powder (97%), and crystalline iodine (99.999%) were used as starting materials. Red phosphorus was purified as described elsewhere [18]. Tin tetraiodide was synthesized according to the literature procedure [25]. For the synthesis of $Sn_{24}P_{19.3}I_8$, a stoichiometric mixture of tin, phosphorus, and tin tetraiodide was sealed under vacuum in a silica tube. The tube was slowly ($10\,K\,h^{-1}$) heated to 775 K, annealed for 5 days, and then cooled with the furnace. After regrinding, the sample was heated at the same conditions for another 5 days. The obtained polycrystalline product was phase-pure according to the profile analysis of the X-ray powder diffraction pattern (STADI-P, Stoe, Cu$K_{\alpha1}$ radiation, Si as an internal standard). The phase identification and the pattern treatment were processed with the WINXPOW program package. The calculated cubic unit cell parameter, $a = 10.950(1)$ Å, was in excellent agreement with the literature data [26]. For the single crystal preparation, the same mixture of the starting materials was annealed at 825 K for 5 days; suitable crystals were selected from the multiphase product.

2.2. Low-temperature X-ray powder diffraction experiments

The angular position of the (0 0 12) reflection, having the Bragg angle θ of about 79°, was measured for the powder sample of $Sn_{24}P_{19.3}I_8$ in the temperature range of 5–301 K using the DRON-7 diffractometer (Co$K_{\alpha1}$ radiation, Si as an external standard) equipped with the home-built helium cryostat. The sample was first cooled down to 5 K, and then the readings were recorded upon heating with the step of 3–5 K to 80 K and further with the step of 7–8 K. Temperature was measured using a copper/iron-chromel thermocouple with the precision of 0.1 K. At each temperature, the peak position was measured at least twice to make sure that the thermal equilibrium is achieved. The accuracy of the unit cell parameter calculation at each temperature was 10^{-4} Å. The detailed description of the experimental setup is given elsewhere [27,28].

2.3. Crystal structure determination

The X-ray intensity data were measured at seven temperatures ranging from 90 to 293 K on a Bruker SMART APEX CCD-based X-ray diffractometer system equipped with a Bruker KRYOFLEX low-temperature attachment and a Mo-target X-ray tube ($\lambda = 0.71073$ Å) operated at 1800 W power. The cubic-shaped crystal with dimensions of 0.05 mm × 0.05 mm × 0.05 mm was mounted on a goniometer head with silicone grease. The detector was placed at a distance of 6.14 cm from the crystal. A total of 1850 frames were collected with a scan width of 0.3° in ω and an exposure time of 20 s/frame. The frames were integrated with the Bruker SAINT software package using a narrow-frame integration algorithm to a maximum 2θ angle of 56.54° (0.75 Å resolution). The final cell constants are based upon the refinement of the *XYZ*-centroids of several thousand reflections above $20\sigma(I)$. Data were corrected for absorption effects using the empirical method (SADABS). The structures were solved and refined by full-matrix least squares procedures on $|F^2|$ using the Bruker SHELXTL (version 6.12) software package. A larger crystal with dimensions of 0.09 mm × 0.08 mm × 0.08 mm was used for the X-ray experiment at 10 K on a Bruker SMART APEX CCD-based X-ray diffractometer system equipped with a helium-flow temperature controller (Japan Thermal Eng. TC-10 KCP) using graphite-monochromated MoK_α radiation ($\lambda = 0.71073$ Å).

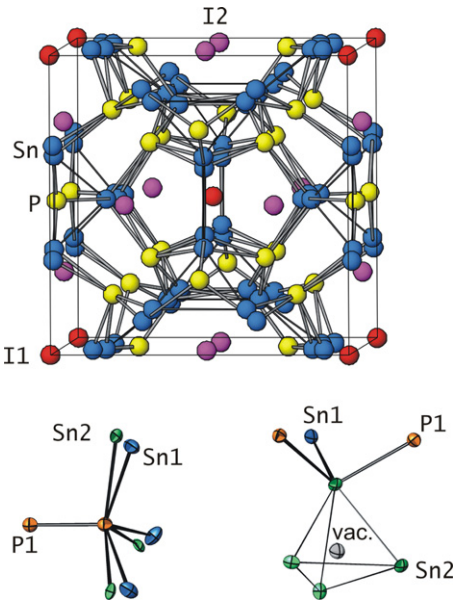

Fig. 1. Crystal structure of $Sn_{24}P_{19.3}I_8$. (top) A view of the unit cell; (bottom) coordination of the P1 (left) and Sn2 (right) atoms; "vac." denotes vacancy in the P2 position.

2.4. Heat capacity measurements

The heat capacity of $Sn_{24}P_{19.3}I_8$ was measured by the absolute adiabatic method with periodical heating in the range of 2.6–300 K using an automated calorimeter made by Termax Inc. The temperature was monitored using an iron-rhodium thermocouple with the precision better than 0.02 K. The systematic error in the heat capacity was about 3% in the temperature range of 2.6–20 K and about 1% between 60 and 300 K.

3. Results and discussion

3.1. Crystal structure and thermal expansion

The crystal structure of $Sn_{24}P_{19.3}I_8$ was refined for 8 different temperatures using the crystal data discussed elsewhere [26] as the initial model. The summary of the crystal data and refinement parameters for all experiments is given in Table 1. Fig. 1 shows the details of the crystal structure. Tin and phosphorus atoms occupy two crystallographic positions each, forming a framework, while guest iodine atoms occupy positions 2*a* and 6*d* at the centers of the large polyhedral cages of 20 and 24 vertices, respectively. Within the framework, only the phosphorus atom at the 16*i* position (P1) has a full occupancy. The phosphorus atom at the 6*c* site (P2) resides only 2.0 Å apart from the tin atom that occupies the 24*k*″ site (Table 2). This distance is too short, meaning that these two atoms alternate. Also alternating are the tin atoms occupying the 24*k*′ (Sn1) and 24*k*″ (Sn2) positions, since the corresponding interatomic distance is ca. 0.6 Å. The two types of tin atoms differ in their coordination with one (Sn1) having the tetrahedral environment typical for clathrate frameworks (Sn1), whereas the other (Sn2) displaying the 3 + 3 coordination. Such a difference in the atomic coordination was previously confirmed by the Mössbauer spectroscopy [29]. The host-guest distances exceed 3.7 Å, pointing to the absence of the covalent host-guest interaction.

Careful examination of the structural details shows that no structural changes, including possible phase transitions, occur upon varying the temperature. In particular, no sign of the 6*d* guest position splitting was found at any temperature. This shows that

Table 1
Crystal structure collection and refinement parameters for $Sn_4P_{19.3}I_8$ at different temperatures; space group *Pm*3-*n*; *Z* = 1; 23 refined parameters.

Data collection temperature (K)	10 (2)	90 (2)	173 (2)	213 (2)	233 (2)	263 (2)	273 (2)	295 (2)
Cell parameter, a (Å)	10.9173 (3)	10.9265 (2)	10.9358 (2)	10.9407 (2)	10.9446 (5)	10.9481 (2)	10.9494 (2)	10.9553 (4)
V, Å^3	1301.21 (6)	1304.50 (4)	1307.83 (4)	1309.59 (4)	1310.99 (9)	1312.25 (4)	1312.72 (4)	1314.84 (8)
Density (calc.) (g cm^{-3})	5.694	5.679	5.665	5.657	5.651	5.646	5.644	5.635
μ (mm^{-1})	16.630	16.588	16.546	16.524	16.506	16.490	16.484	16.458
2θ (max),°	28.22	28.26	28.24	28.22	28.29	28.28	28.27	28.26
Reflections collected	8695	10,168	10,209	10,241	10,230	10,233	10,255	10,116
Independent reflections	318	319	320	320	320	322	322	320
R_{int}	0.0355	0.0212	0.0213	0.0216	0.0223	0.0212	0.0227	0.0263
R_1 (all data) and wR_2 (all data)	0.0235 0.0442	0.0196 0.0395	0.0199 0.0382	0.0194 0.0374	0.0207 0.0396	0.0208 0.0397	0.0203 0.0387	0.0205 0.0383
Goodness-of-fit	1.379	1.489	1.447	1.454	1.432	1.453	1.412	1.401
Largest diff. peak and hole (e/Å^3)	0.73, −0.87	0.69, −0.73	0.55, −0.59	0.62, −0.69	0.68, −0.76	0.52, −0.53	0.52, −0.63	0.59, −0.55

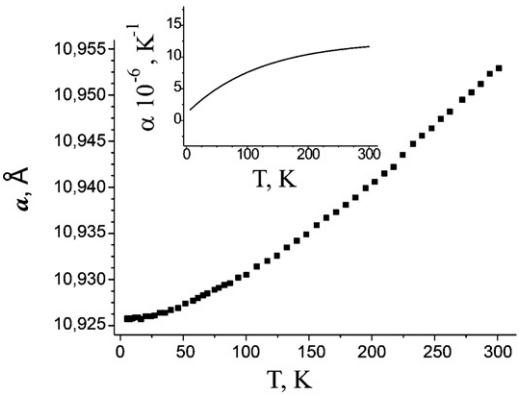

Fig. 2. Unit cell parameter of $Sn_{24}P_{19.3}I_8$ as a function of temperature according to the powder diffraction data. The inset shows the temperature dependence of the linear thermal expansion coefficient for $Sn_{24}P_{19.3}I_8$.

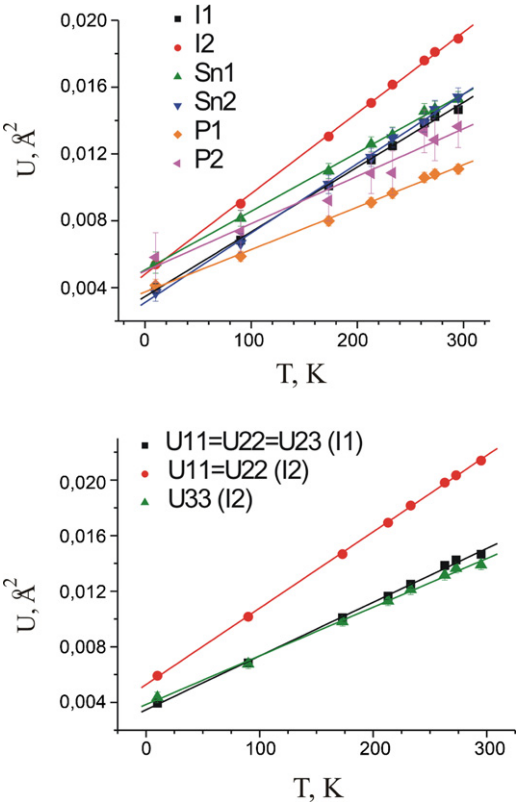

Fig. 3. Temperature dependence of the ADP's for $Sn_{24}P_{19.3}I_8$. (top) Equivalent ADP's for all atoms. (bottom) Guest atom ADP's in an anisotropic mode. Note that for some points the size of the error bar is smaller than the size of the respective symbol.

cationic clathrates behave differently compared to their anionic counterparts, for which the splitting of the 6*d* site into 12-fold or 24-fold positions is rather the norm than the exception [13].

The unit cell of $Sn_{24}P_{19.3}I_8$ contracts upon cooling (Fig. 2). It decreases almost linearly down to 150 K, after which the unit cell parameter diminishes with less increment. The linear thermal expansion parameter calculated as $\alpha = \{[a(T_1) - a(T_2)]/a(T_2)\}/(T_1 - T_2)$, where a is a cubic unit cell parameter at a temperature $T_1 > T_2$, shows a distinct variation with temperature. Within the range of 200–300 K, α takes an average value of 11.1×10^{-6} K^{-1}, which is similar to the value observed for the bromine analog and, furthermore, is typical for the tin-based type-I clathrates [30]. The contraction of the structure is accompanied by only minor changes in the bond distances. For instance, the P1–P1 bond length does not change within the accuracy of the determination, whereas the Sn2–Sn2 distance decreases by 0.02 Å upon cooling from 293 to 10 K. Noticably, the unit cell parameters obtained from the X-ray powder diffraction data differ at low temperature from those obtained from the X-ray single-crystal diffraction data, the difference becoming more pronounced upon approaching helium temperatures. This type of behavior was previously reported for several clathrate compounds but received no sound explanation [30,31].

3.2. Atomic displacement and characteristic temperatures

Top panel of Fig. 3 shows the temperature dependence of the equivalent atomic displacement parameters (ADP) for all atoms in the crystal structure of $Sn_{24}P_{19.3}I_8$. The dependence is linear

Table 2
Atomic parameters for $Sn_{24}P_{19.3}I_8$ at 10 K.

Atom	Site	*x*/*a*	*y*/*b*	*z*/*c*	U (eq) × 10^4 (Å)	Sof[a]
I1	2*a*	0	0	0	40 (3)	1
I2	6*d*	0	0.25	0.5	54 (2)	1
Sn1	24*k*′	0.3868 (3)	0.1913 (2)	0.5	55 (4)	0.548 (8)
Sn2	24*k*″	0.3467 (3)	0.1566 (3)	0.5	37 (5)	0.452 (8)
P1	16*i*	0.1919 (1)	0.1919 (1)	0.1919 (1)	41 (4)	1
P2	6*c*	0	0.5	0.25	58 (13)	0.548 (8)

[a] "Sof" is a site occupancy factor.

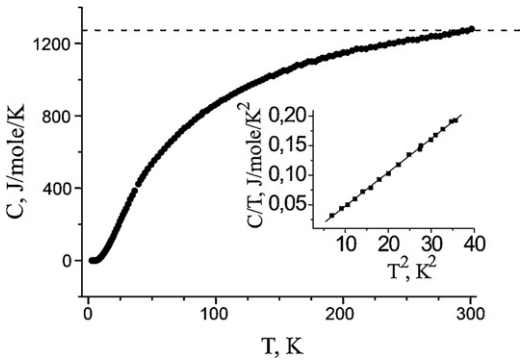

Fig. 4. Heat capacity as a function of temperature for $Sn_{24}P_{19.3}I_8$; the Dulong–Petit value for $Sn_{24}P_{19.3}I_8$ is shown as a dashed line; the inset shows the dependence of C_p/T versus T^2 at $T < 6.5$ K.

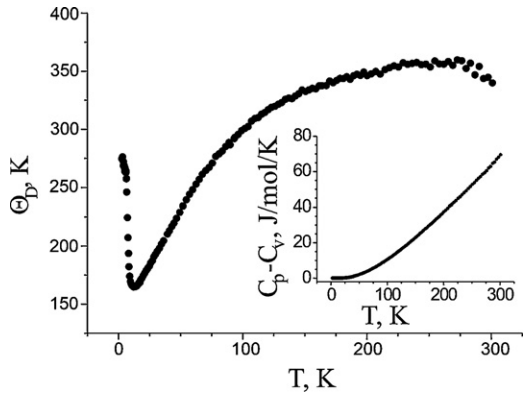

Fig. 5. Plot of θ_D versus T; the inset shows the $C_p - C_v$ difference versus temperature.

and clearly the ADP for the I2 atom is the largest of all at any temperature. The linear dependencies of the ADP's for all atoms were used for estimation of the Debye temperature, θ_D. Taking into account that the slope of the $\langle u^2 \rangle = f(T)$ function is expressed as $3h^2/(4\pi^2 M\theta_D{}^2 k_B)$, where M is the average atomic mass and $\langle u^2 \rangle$ is the mean square atomic displacement [32], we obtained $\theta_D = 225$ K, which is close to the value of $\theta_D = 220$ K calculated previously for the bromine analog using the analogous procedure [18]. This finding is not surprising taking into account that two compounds have the same composition and structure of the framework and only differ by the nature of the guest atoms, which brings about the mass difference of 8%; therefore their phonon spectra should be similar.

The Debye temperature reflects the lattice dynamics, whereas the motion of the guest atoms can be described in terms of the Einstein model [33]. Accordingly, the guest atoms oscillate with the characteristic Einstein temperature, θ_E, independent of the collective motion of the framework atoms. There are two guest atoms in the structure of $Sn_{24}P_{19.3}I_8$, and their motion is different. It is isotropic ($U_{11} = U_{22} = U_{33}$) for I1, whereas I2 has two directions of motion. The equatorial movement is described by the $U_{11} = U_{22}$ components whereas the axial movement is defined by the U_{33} component. The temperature dependencies of these components are shown in Fig. 3 (bottom). From these linear dependencies the θ_E values were calculated; it is known from the literature that the slope of the $\langle u_{ii} \rangle = f(T)$ function is equal to $[\hbar^2/(2mk_B\theta_E)]\coth(\theta_E/2\pi)$ [34]. The resulting values are $\theta_E(U_{11} = U_{22}) = 63$ K and $\theta_E(U_{33}) = 79$ K for I2 and $\theta_E(U_{11}) = 76$ K for I1. Apparently, the latter two temperatures are nearly the same, as expected from the corresponding dependencies shown in the bottom panel of Fig. 3.

3.3. Heat capacity and lattice dynamics

Fig. 4 shows the heat capacity for $Sn_{24}P_{19.3}I_8$ versus temperature in the range of 2–300 K. Clearly, no anomaly indicative of a phase transition is seen, which corroborates the crystal structure data. Close to 300 K, $C_p(T)$ saturates and reaches the Dulong–Petit value of 1278.9 J mol^{-1} K^{-1} calculated for 51.3 atoms per formula. The inset on Fig. 4 represents the low-temperature part of the C_p/T versus T^2 plot (for $T < 6.5$ K). From a linear fit to C_p/T vs. T^2 the electronic heat capacity was estimated to be $C_{el} = 0.0057 \cdot T$ J mol^{-1} K^{-1}. Such a low value is typical for semiconductors; indeed, as we reported previously [35], $Sn_{24}P_{19.3}I_8$ is a narrow-gap semiconductor with $E_a = 18$ meV. The slope of this fit enabled us to calculate the Debye temperature at 0 K using the Debye-T^3 law, $C_v = [(12R\pi^4)/5] \cdot (T/\theta_D)^3$. The obtained value of $\theta_D = 265$ K differs from that calculated from the crystal data ($\theta_D = 225$ K). We believe that the former value is reliable, whereas the application of the Debye model for calculating θ_D from the crystal data introduces significant inaccuracy because this model implies that a cubic unit cell consists of atoms of only one kind [36]. The isochoric heat capacity, C_v, was calculated using the relation $C_p - C_v = AC_p{}^2T$ with $A = 1.43 \times 10^{-7}$ mol J^{-1} obtained assuming that at the temperature of $T = \theta_D/3$ the following condition applies, $(C_p - C_v)/C_p = 0.01$ [37]. Though the difference between the C_p and C_v values is almost negligible at low temperatures, it reaches 69.5 J mol^{-1} K^{-1} at 300 K. The isochoric heat capacity was used for the accurate calculation of the temperature dependence of θ_D (Fig. 5). It shows a pronounced minimum at around 20 K; therefore, the character of the $\theta_D(T)$ function itself shows that the Debye model cannot describe satisfactorily the temperature dependence of the heat capacity for $Sn_{24}P_{19.3}I_8$.

Fig. 6 shows a plot of C_v/T^3 versus T^2, which reveals a broad maximum at around 12.5 K. From this maximum, a value of $\theta_E = 63$ K is obtained considering that an Einstein contribution shows up in this type of plot as a maximum at $0.2\theta_E$, whereas the Debye contribution is constant at low temperatures [36,38]. It is noticeable that the obtained θ_E is the same as the one calculated from the crystal data for the equatorial motion of the I2 atom. However, the crystal data indicate that there should be two different Einstein temperatures. This was taken into account for the analysis of the $C_v(T)$ function for $Sn_{24}P_{19.3}I_8$, which was treated as the sum of one Debye and two Einstein terms. The general dependence of the heat capacity versus temperature is given as $C_v(T) = C_D(T) + (g/t)C_E(T)$, where C_D and C_E are the Debye and Einstein contributions, g is the number of the guest iodine atoms per formula, and t is the total number of atoms in the unit cell [39]. There are two types of the guests in the crystal structure present in the 1/3 ratio and having different Einstein temperatures, θ_{E1} and θ_{E2}. At the first approximation $\theta_{E1}/\theta_{E2} = U_2/U_1$, where $U_1 = 0.0127$ and $U_2 = 0.0167$ [19] are the equivalent displacement parameters for I(1) and I(2) atoms, respectively. To account for the contribution of two different guest atoms the coefficients a_1 and

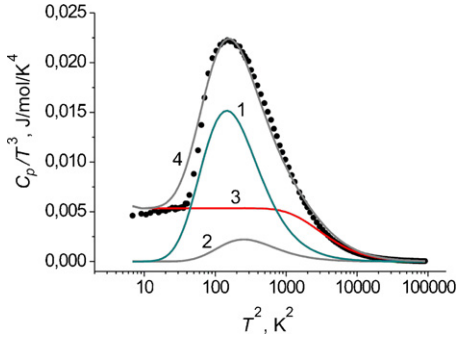

Fig. 6. Plot of C_P/T^3 versus T^2 in semi-logarithmic coordinates. Two Einstein (1, 2) and one Debye (3) contributions to the total C_p/T^3 values (4) are given in comparison with the experimental data (filled circles).

a_2, were introduced such that $a_1 + a_2 = g/t = 0.156$ and $a_1/a_2 = 1/3$. Accordingly, $a_1 = 0.039$ and $a_2 = 0.117$. This gave the equation $C_v(T) = C_D(265/T) + 0.039\,C_E(\theta_{E1}/T) + 0.117\,C_E(\theta_{E2}/T)$, for which the resulting least-squares fit yielded two Einstein temperatures, $\theta_{E1} = 60$ K and $\theta_{E2} = 78$ K. With these values and $\theta_D = 265$ K, the calculated C_p/T^3 versus T^2 dependence describes nicely the experimental data (Fig. 6), with some discrepancy noticeable at temperatures below 4 K, which is typical for these kind of fits [40,41]. Again, the obtained values of θ_E are close to those calculated from the crystal data (*above*). This confirms that both models satisfactory describe the pseudo-localized motion of the guest atoms inside the oversized cages and that the host-guest interaction is weak enough and allows treating the rattling of the guests independently of the collective motion of the framework atoms. Besides, such a good matching of the θ_E values obtained with the use of two different methods provides an indirect proof for the crystal structure model involving no disorder for the guest atoms in the larger cavity. It is known from the literature that the difference in θ_E can reach 20 K if the existing guest disorder is ignored [42,43].

3.4. Lattice part of the thermal conductivity

The lattice part of the thermal conductivity of a solid can be estimated from the Debye equation for thermal conductivity, $\kappa_L = 1/3(C \cdot v_s \cdot \lambda)$, where C is the heat capacity per unit volume, v_s is the mean phonon velocity, and λ is the phonon mean free path [36]. Given the Debye temperature of 265 K, the mean phonon velocity can be calculated as $v_s = (k_B \cdot \theta_D/\hbar) \cdot [6\pi^2(N/V)]^{-1/3} = 2627\ \mathrm{m\,s^{-1}}$. The value of the volume heat capacity derived from the experimentally obtained C_p value and X-ray density at 293 K is $1.65\ \mathrm{J\,m^{-3}\,K^{-1}}$. Finally, the phonon mean free path was taken as the average separation (6.1×10^{-10} m) of the rattling guest atoms, which motion presumably scatters heat-carrying phonons. The obtained room-temperature value of $\kappa_L = 0.85\ \mathrm{W\,m^{-1}\,K^{-1}}$ can be compared with that observed experimentally [19,35]. The latter was reported to exceed $1\ \mathrm{W\,m^{-1}\,K^{-1}}$ at room temperature; however, careful inspection of the literature data suggests that the room temperature value is affected by the radiation losses inherent in measurement of the samples with low thermal conduction employing the steady-state method. From the reported experimental data the minimal value observed at about 150 K is roughly estimated as $0.9\ \mathrm{W\,m^{-1}\,K^{-1}}$. We believe that this value can be considered as the intrinsic room-temperature total thermal conductivity of $Sn_{24}P_{19.3}I_8$, which is quite comparable with our estimations.

The total thermal conductivity is a sum of the lattice and electronic contributions. The latter can be estimated using the Wiedemann–Franz law, which relates the electrical (σ) and thermal conductivity for metals, $\kappa_e = \sigma \cdot L_0 \cdot T$, where L_0 is the ideal Lorentz number $L_0 = 2.45 \times 10^{-8}\ \mathrm{W\,\Omega\,K^{-2}}$ [36]. Given the room temperature electrical conductivity of $Sn_{24}P_{19.3}I_8$, $\sigma = 1650\ \mathrm{S\,m^{-1}}$ [35], we estimate the electronic part of the thermal conductivity as $\kappa_e = 0.01\ \mathrm{W\,m^{-1}\,K^{-1}}$, which constitutes slightly over 1% of the total thermal conductivity. Therefore, the thermal conductivity of $Sn_{24}P_{19.3}I_8$ can be described as the dominate contribution of the lattice part arising from the localized motion of the guest atoms.

4. Conclusions

The crystal structure of the cationic clathrate $Sn_{24}P_{19.3}I_8$ shows no variations down to 10 K. Even at this temperature, no sign of positional disorder in the guest substructure is observed, which is in contrast with the typical behavior of the anionic clathrates where the guest positions are described using the split model. The results of the heat capacity measurements for $Sn_{24}P_{19.3}I_8$ cannot be rationalized within the Debye model for thermal conductivity of solids and point to the presence of the localized vibrations of the guest atoms. Both the crystal structure data and the heat capacity measurements give nearly the same Einstein temperatures characteristic of the guest motion inside the framework cavities; consequently, the heat capacity of $Sn_{24}P_{19.3}I_8$ is described using two Einstein and one Debye terms with the corresponding characteristic temperatures of $\theta_{E1} = 60$ K, $\theta_{E2} = 78$ K, and $\theta_D = 265$ K. The lattice and electronic parts of the thermal conductivity of $Sn_{24}P_{19.3}I_8$ calculated using the experimental and literature data reveal that the low thermal conductivity of the cationic clathrate is almost entirely phononic, $\kappa_L = 0.85\ \mathrm{W\,m^{-1}\,K^{-1}}$, and is derived from the localized motion of the guest atoms inside the polyhedral cages.

Acknowledgments

We thank Prof. K.A. Kovnir for discussion. The support of the Russian Foundation for Basic Research (grant # 10-03-00277) is gratefully acknowledged.

Appendix A. Supplementary data

Supplementary data associated with this article can be found, in the online version, at doi:10.1016/j.jallcom.2011.12.171.

References

[1] T.M. Tritt, H. Böttner, L. Chen, MRS Bull. 33 (2008) 366–368.
[2] G.S. Nolas, in: D.M. Rowe (Ed.), CRC Thermoelectric Handbook 2006 – From Macro to Nano, Taylor & Francis Group, LLC, Boca Raton, 2006 (Chapter 33).
[3] A.V. Shevelkov, Usp. Khim. 77 (2008) 3–21, Russ. Chem. Rev. 77 (2008) 1–19.
[4] M.S. Dresselhaus, G. Chen, M.Y. Tang, R.G. Yang, H. Lee, D.Z. Wang, Z.F. Ren, J.-P. Fleurial, P. Gogna, Adv. Mater. 19 (2007) 1043–1053.
[5] J.R. Sootsman, D.Y. Chung, M.G. Kanatzidis, Angew. Chem. Int. Ed. 48 (2009) 8616–8639.
[6] M.A. McGuire, T.J. Scheidemantel, J.V. Badding, F.J. DiSalvo, Chem. Mater. 17 (2005) 6186–6191.
[7] N. Eckstein, T. Nilges, R. Decourt, J.-L. Bobet, B. Chevalier, J. Solid State Chem. 184 (2011) 778–785.
[8] J.V. Zaikina, K.A. Kovnir, A.V. Sobolev, I.A. Presniakov, Yu. Prots, M. Baitinger, W. Schnelle, A.V. Olenev, O.I. Lebedev, G. van Tendeloo, Yu. Grin, A.V. Shevelkov, Chem. Eur. J. 13 (2007) 5090–5099.
[9] K. Salzgeber, P. Prenninger, A. Grytsyv, P. Rogl, E. Bauer, J. Electron. Mater. 39 (2010) 2074–2078.
[10] A.V. Shevelkov, K. Kovnir, Struct. Bond. 139 (2011) 97–142.
[11] G.A. Jeffrey, in: J.L. Atwood, J.E.D. Davies, D. MacNichol (Eds.), Hydrate Inclusion Compounds in Inclusion compounds, Academic Press, London, 1983, p. P135.
[12] M.A. Kirsanova, A.V. Olenev, A.M. Abakumov, M.A. Bykov, A.V. Shevelkov, Angew. Chem. Int. Ed. 50 (2011) 2371–2374.
[13] M. Christensen, S. Johnsen, B.B. Iversen, Dalton Trans. 39 (2010) 978–992.
[14] J.V. Zaikina, K.A. Kovnir, U. Burkhardt, W. Schnelle, F. Haarmann, U. Schwarz, Yu. Grin, A.V. Shevelkov, Inorg. Chem. 48 (2009) 3720–3730.
[15] K. Kishimoto, T. Koyanagi, K. Akai, M. Matsuura, Jpn. J. Appl. Phys. 46 (2007) L746–L748.
[16] K. Kishimoto, S. Arimura, T. Koyanagi, Appl. Phys. Lett. 88 (2006) 222115.
[17] M.A. Kirsanova, L.N. Reshetova, A.V. Olenev, A.M. Abakumov, A.V. Shevelkov, Chem. Eur. J. 17 (2011) 5719–5726.
[18] K.A. Kovnir, J.V. Zaikina, L.N. Reshetova, A.V. Olenev, E.V. Dikarev, A.V. Shevelkov, Inorg. Chem. 43 (2004) 3230–3236.
[19] J.V. Zaikina, W. Schnelle, K.A. Kovnir, A.V. Olenev, Yu. Grin, A.V. Shevelkov, Solid State Sci. 9 (2007) 664–671.
[20] M. Falmbigl, P.F. Rogl, E. Bauer, M. Kriegisch, H. Müller, S. Paschen, Mater. Res. Soc. Symp. Proc. 1166 (2009), N06–03.
[21] K.A. Kovnir, M.M. Shatruk, L.N. Reshetova, I.A. Presniakov, E.V. Dikarev, M. Baitinger, F. Haarmann, W. Schnelle, M. Baenitz, Yu. Grin, A.V. Shevelkov, Solid State Sci. 7 (2005) 957–968.
[22] A.V. Shevelkov, M.M. Shatruk, Russ. Chem. Bull. 50 (2001) 337–352.
[23] M. Christensen, A.B. Abrahamsen, N.B. Christensen, F. Juranyi, N.H. Andersen, K. Lefmann, J. Andreasson, C.R.H. Bahl, B.B. Iversen, Nat. Mater. 7 (2008) 811–815.
[24] T. Tanaka, T. Onimaru, K. Suekuni, S. Mano, H. Fukuoka, S. Yamanaka, T. Takabatake, Phys. Rev. B 81 (2010) 165110.
[25] G. Brauer, Handbuch der Präparativen Anorganischen Chemie Ed, Ferdinand Enke Verlag, Stuttgart, 1975.
[26] M.M. Shatruk, K.A. Kovnir, A.V. Shevelkov, I.A. Presniakov, B.A. Popovkin, Inorg. Chem. 38 (1999) 3455–3457.
[27] N.N. Sirota, V.V. Novikov, A.V. Novikov, Phys. Solid State 42 (2000) 2033–2035.
[28] N.N. Sirota, V.V. Novikov, V.A. Vinokurov, Yu.B. Paderno, Phys. Solid State 40 (1998) 1856–1858.

[29] K.A. Kovnir, A.V. Sobolev, I.A. Presniakov, O.I. Lebedev, G. Van Tendeloo, W. Schnelle, Yu. Grin, A.V. Shevelkov, Inorg. Chem. 44 (2005) 8786–8793.
[30] M. Falmbigl, G. Rogl, P. Rogl, M. Kriegisch, H. Müller, E. Bauer, M. Reinecker, W. Schranz, J. Appl. Phys. 108 (2010) 043529.
[31] B.C. Chakoumakos, B.C. Sales, D.G. Mandrus, G.S. Nolas, J. Alloys Compd. 296 (2000) 80–86.
[32] B.C. Sales, B.C. Chakoumakos, D. Mandrus, J.W. Sharp, J. Solid State Chem. 146 (1999) 528–532.
[33] B.C. Sales, B.C. Chakoumakos, R. Jin, J.R. Thompson, D. Mandrus, Phys. Rev. B 63 (2001) 245113.
[34] J.D. Dunitz, V. Schomaker, K.N. Trueblood, J. Phys. Chem. 92 (1998) 856–867.
[35] A.V. Yakimchuk, J.V. Zaikina, L.N. Reshetova, L.I. Ryabova, D.R. Khokhlov, A.V. Shevelkov, Low Temp. Phys. 33 (2007) 276–279.
[36] M.A. White, Properties of Materials, Oxford University Press, Oxford, 1999.
[37] A. Tari, The Specific Heat of Matter at Low Temperatures, Imperial College Press, London, 2003, 191 pp.
[38] K. Kovnir, U. Stockert, S. Budnyk, Yu. Prots, M. Baitinger, S. Paschen, A.V. Shevelkov, Yu. Grin, Inorg. Chem. 50 (2011) 10387–10396.
[39] W.N. Lawless, Phys. Rev. B 14 (1976) 134–143.
[40] M.K. Drulis, H. Drulis, A.E. Hackemer, A. Ganguly, T. El-Raghy, M.W. Barsoum, J. Alloys Compd. 433 (2007) 59–62.
[41] G.D. Khattak, H. Akbarzadeh, P.H. Keesom, Phys. Rev. B 23 (1981) 2911–2915.
[42] M. Christensen, N. Lock, J. Overgaard, B.B. Iversen, J. Am. Chem. Soc. 128 (2006) 15657–15665.
[43] M. Christensen, B.B. Iversen, Chem. Mater. 19 (2007) 4896–4905.